Coupling Smoothed Particle Hydrodynamics and Reduced Order Heat Transfer for Efficient Casting Simulation

J. Lienemann, I. Cenova, D. Kauzlaric, A. Greiner, Jan G. Korvink
University of Freiburg, Germany

Corresponding author: J. Lienemann, University of Freiburg, Department of Microsystems Engineering (IMTEK), 79110 Freiburg, Georges-Köhler-Allee 103, Germany, [redacted]

Abstract. Casting simulation for microscale components requires multiscale modeling of the heat exchange between the melt and the macroscopic mould, the results allowing for detection of early solidification and the calculation of cooling curves.

The melt model, discretized with smoothed particle hydrodynamics (SPH), is coupled to a small ordinary differential equation (ODE) system representing the mould. It is obtained from the model order reduction (MOR) of a finite element method (FEM) discretized system. In this way, the advantages of the Lagrangian discretization of the fluid can be combined with the potential of a spatially refined FEM grid while keeping the requirements on computational ressources low.

1 Introduction

Microcasting is a metal forming process based on lost-wax lost-mold investment casting. It is used to create small structures in the micrometer range by using a metal melt which is cast into a microstructured mold, allowing for very complicated parts even with undercuts. Fields of application are, e.g., instruments for minimal invasive surgery, dental devices and instruments for biotechnology [1].

The process parameters have a large influence on the casting results. Especially in the micro range, solidification may occur before the mold is filled completely, and long structures with small diameters could clog. The reason is that the melt may be cooled below its liquidus temperature too early due to the contact with the colder mold. It is thus imperative to preheat the mold, yet temperatures should remain as low as possible to save processing time and energy. Further, the cooling curve determines the size and shape of grains in the microstructure of an alloy, where grains may reach the size of the micro structure's features. Simulation is used to estimate the cooling curves and to optimize process parameters [2].

One challenge for numerical simulation is the multiscale problem of micrometer sized device features in a centimeter-sized mold. By simulating the thermal behavior of the mold with FEM, a fixed (Eulerian) grid approach with fixed neighborhood relationships, we can use a locally refined mesh close to the micro structures. Since the FEM system of equations is rather large, model order reduction [3] is applied for reducing computation time. The particle method SPH, a Lagrangian discretization of the Navier Stokes equations where neighborhood relationships are calculated on-the-fly, is used for the fluid. It allows for a convenient simulation of free surfaces and internal degrees of freedom (DOFs) like enthalpy, since the discretization moves along with the flow. Exchange of thermal energy and thus coupling of FEM and SPH is achieved by special terminal particles on the wall. Figure 1 shows a schematic outline.

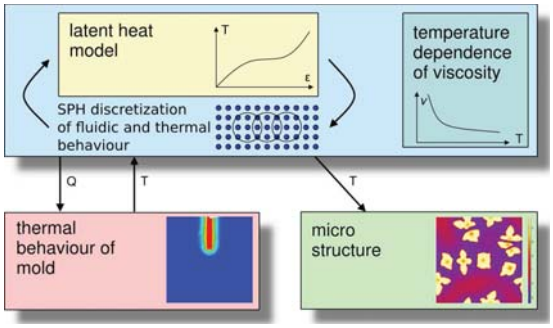

Figure 1: Schematic outline of the simulation process

The simulation geometry consists mainly of the sprue, the microstructures are attached at the bottom. The melt is poured in to the system from the top (Fig. 2). It is initially formed as a cube of SPH particles with side length 8 mm and positioned just above the two sprue channels. Being at rest at the beginning of the simulation, gravity accelerates it (acceleration by centrifugal force can easily be implemented, too).

The rest of the paper is organized as follows: Section 2 discusses the finite element method with a special focus on input and output terminals on the FEM domain's boundaries. Section 3 presents model order reduction by moment

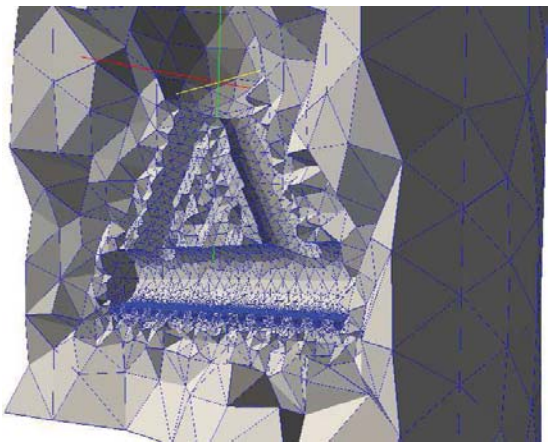

Figure 2: Computational mesh of the mold used for FEM. Diameter: 47 mm, height: 55 mm

matching. Section 4 shows how the SPH discretisation is applied to the casting model. Section 5 shows how those methods can be combined in an integrated model. Finally, section 6 presents results obtained with the model.

2 The Finite Element Method and its interfaces

Let the simulation domain $\Omega \subset \mathbb{R}^3$ be an open set with piecewise smooth boundary $\Gamma = \overline{\Gamma_q \cup \Gamma_h}$, furthermore let $\overline{\Gamma_q \cap \Gamma_h} = \emptyset$, where the bar means the set closure. Let $\boldsymbol{n}$ be the unit outward normal vector to Γ, c the specific heat, ρ the mass density and κ the thermal conductivity of the melt; those values shall be positive and, in contrast to the fluid, constant for the mold. We seek the solution of the heat transfer equation for the temperature T at time $t > t_0$,

$$\nabla \cdot (\kappa \nabla T) - c\rho \frac{\partial T}{\partial t} = 0 \qquad \text{in } \Omega$$

with boundary and initial conditions $T = q$ on Γ_q, $-\kappa \nabla T \cdot \boldsymbol{n} = h$ on Γ_h, and $T(t = t_0) = T_0$ in $\overline{\Omega}$. After building the weighted residual with weighting functions $\theta_i \in H^1(\overline{\Omega})$ the equation is transformed to the weak form by partial integration. The temperature is now approximated by shape functions φ_i, so that $T = \sum_j T_j(t)\varphi_j(\boldsymbol{r})$. In the Galerkin FEM, $\varphi_i = \theta_i$.

$$\sum_j \dot{T}_j \int_\Omega c\rho\, \varphi_j \theta_i \,\mathrm{d}v + \sum_j T_j \int_\Omega \kappa \nabla \varphi_j \nabla \theta_i \,\mathrm{d}v = \int_\Gamma \kappa \nabla T \cdot \boldsymbol{n}\, \theta_i \,\mathrm{d}\Gamma \tag{1}$$

For the coupling process, we need to access temperature data $\hat{T}_k$ at several locations $\boldsymbol{r}_k$ using the shape functions, $\hat{T}_k = \sum_j T_j(t)\varphi_j(\boldsymbol{r}_k)$; the resulting multiplication factors for the T_j can be computed in advance, resulting in $\hat{\boldsymbol{T}} = \mathbf{C}\boldsymbol{T}$, where $\mathbf{C}$ is the output matrix.

The model order reduction approach we use depends on the definition of a limited number of system inputs, where each additional input has an impact on the total size of the reduced system.

The inner wall of the mould, which is in contact to the melt, is partitioned into surface patches Γ_l (see Fig. 4). The heat flux from the melt into the mould is averaged on such a patch. Assume that the averaged flux is $-\kappa \nabla T \cdot \boldsymbol{n} = J_l$, then the contribution to the right-hand side of (1) is

$$f_i = \int_\Gamma -J(\boldsymbol{r})\, \theta_i \,\mathrm{d}\Gamma = \sum_l \int_{\Gamma_l} -J_l \theta_i \,\mathrm{d}\Gamma = \sum_l B_{il} J_l.$$

We call $\mathbf{B}$ the input matrix of the system. In this way, we define input and output terminals and matrices for the system, so that the linear system composed from (1) reads

$$\begin{aligned} \mathbf{E}\dot{\boldsymbol{T}} &= \mathbf{A}\boldsymbol{T} + \mathbf{B}\boldsymbol{J} \\ \hat{\boldsymbol{T}} &= \mathbf{C}\boldsymbol{T}. \end{aligned} \tag{2}$$

3 Model Order Reduction

Model order reduction is used to generate a compact model of the thermal behavior of the mold automatically [3, 4], since the complexity of FEM models like (2) results in long CPU simulation times.

The system of equations is converted to frequency space by a Laplace transform, $\tilde{T} = \mathscr{L}(T), \tilde{J} = \mathscr{L}(J)$:

$$\begin{aligned} s\mathbf{E}\tilde{\boldsymbol{T}}(s) - \mathbf{A}\tilde{\boldsymbol{T}}(s) &= \mathbf{B}\tilde{\boldsymbol{J}}(s) \\ \tilde{\hat{\boldsymbol{T}}}(s) &= \mathbf{C}\tilde{\boldsymbol{T}}(s). \end{aligned}$$

The transfer function of the system and its Taylor expansion are:

$$\begin{aligned}\mathbf{H}(s) &= \tilde{\tilde{\boldsymbol{T}}}/\tilde{\boldsymbol{J}} \\ &= \mathbf{C}\left(s\mathbf{E}-\mathbf{A}\right)^{-1}\mathbf{B} \\ &= \mathbf{C}\left(s\mathbf{A}^{-1}\mathbf{E}-\mathbf{I}\right)^{-1}\mathbf{A}^{-1}\mathbf{B} \\ &= \sum_{i}^{\infty} s^i \Big[-\mathbf{C}\underbrace{\left(\mathbf{A}^{-1}\mathbf{E}\right)^i\mathbf{A}^{-1}\mathbf{B}}_{\mathbf{m}_i}\Big].\end{aligned}$$

The goal of moment matching methods is a reduced system $\mathbf{E}_r\dot{\boldsymbol{T}}_r(t) = \mathbf{A}_r\boldsymbol{T}_r(t) + \mathbf{B}_r\boldsymbol{J}(t)$; $\hat{\boldsymbol{T}}(t) = \mathbf{C}_r\boldsymbol{T}_r(t)$, where the first q moments of the Taylor expansion of the transfer functions of the full and the reduced system are equal. For that purpose, the *moments* $\mathbf{m}_1,\ldots,\mathbf{m}_q$ with $\mathbf{m}_i = \left(\mathbf{A}^{-1}\mathbf{E}\right)^i\mathbf{A}^{-1}\mathbf{B}$ are used as basis vectors for a subspace $\mathbf{V}$ such that $\boldsymbol{T} \approx \mathbf{V}\boldsymbol{T}_r$. Using this projection in (2) and left-multiplying the first line with $\mathbf{V}^T$ results in

$$\begin{aligned}\mathbf{E}_r &= \mathbf{V}^T\mathbf{E}\mathbf{V} & \mathbf{A}_r &= \mathbf{V}^T\mathbf{A}\mathbf{V} \\ \mathbf{B}_r &= \mathbf{V}^T\mathbf{B} & \mathbf{C}_r &= \mathbf{C}\mathbf{V}.\end{aligned} \tag{3}$$

and the corresponding system

$$\begin{aligned}\mathbf{E}_r\dot{\boldsymbol{T}}_r &= \mathbf{A}_r\boldsymbol{T}_r + \mathbf{B}_r\boldsymbol{J} \\ \hat{\boldsymbol{T}} &= \mathbf{C}_r\boldsymbol{T}_r.\end{aligned}$$

The basis vectors of the subspace are calculated iteratively, $\boldsymbol{v}_{i+1} = \left(\mathbf{A}^{-1}\mathbf{E}\right)\boldsymbol{v}_i$ (*Krylov subspace*). Since the explicit calculation of moments leads to numerical instabilities, in the *Arnoldi* algorithm these moments are orthonormalized by a modified Gram-Schmidt procedure [11]. Often, results are already satisfactory for small q (e.g., 5 per input). However, it is necessary to limit the model to a low number of external inputs, since every input enlarges the number of reduced variables.

The size of the reduced system can be selected independently from the size of the original system, so that even highly-resolved full systems can be reduced to a few degrees of freedom.

4 Smoothed Particle Hydrodynamics

The SPH method has its basis in astronomy, where it was applied to the simulation of galaxies, but it is flexible enough to bridge the gap to the microsystem range. In contrast to FEM and when used for fluidic simulation, SPH is a Lagragian discretization (moving along with the flow); neighborhood relationships are calulated on-the-fly. It is very useful for large deformations, free surfaces, where the fluid part is represented by the presence of particles, and for contact problems. Each particle may carry additional degrees of freedom (DoFs), and those DoFs are automatically transported along, so that no convection equations such as for the Eulerian methods need to be solved. The starting point of SPH is the idea that an arbitrary function $f(\boldsymbol{r})$ may be approximated by [5, 6]

$$\langle f(\boldsymbol{r})\rangle \approx \int f\left(\boldsymbol{r}'\right) W_h\left(\boldsymbol{r}-\boldsymbol{r}'\right)\,\mathrm{d}\boldsymbol{r}'$$

where $W_h(\boldsymbol{r}-\boldsymbol{r}')$ is an interpolation function of width h which is normalized by $\int_{\mathbb{R}^n} W\,\mathrm{d}v = 1$. The integral is replaced by a sum over a finite number of material points or "particles" at position $\boldsymbol{r}_j$. Additionally we replace $f(\boldsymbol{r})$ by the particle-centered value $f_i = f(\boldsymbol{r}_i)$, where i is the particle index. Using m_j for the particle mass, ρ_j for the particle's local density and $W_{ij} = W_h(\boldsymbol{r}_i-\boldsymbol{r}_j)$, we find for $\langle f_i\rangle$ and its spatial derivative:

$$\begin{aligned}\langle f_i\rangle &\approx \sum_{j\neq i}\frac{m_j}{\rho_j}f_jW_{ij} \\ (\nabla f)_i &\approx \sum_{j\neq i}\frac{m_j}{\rho_j}f_j\nabla W_{ij}.\end{aligned}$$

The second derivative can be discretized using the form

$$\begin{aligned}(\nabla\cdot\kappa(\boldsymbol{r})\nabla f)_i &\approx \sum_{j\neq i}\frac{m_j}{\rho_j}\frac{(\kappa_i+\kappa_j)(f_i-f_j)(\boldsymbol{r}_i-\boldsymbol{r}_j)}{\left|\boldsymbol{r}_i-\boldsymbol{r}_j\right|^2}\nabla W_{ij} \\ &= \sum_{j\neq i}\frac{m_j}{\rho_j}(\kappa_i+\kappa_j)(f_j-f_i)F_{ij}\end{aligned}$$

where F_{ij} is defined by $\nabla W_{ij} = -(\boldsymbol{r}_i - \boldsymbol{r}_j) F_{ij}$. The local density can be determined by setting $f = \rho$. Applied to the Lagrangian form of the momentum equation,

$$\frac{\mathrm{d}\boldsymbol{v}}{\mathrm{d}t} = (1/\rho)\nabla\cdot\sigma = -\frac{1}{\rho}\nabla p + \frac{1}{\rho}\nabla\cdot\mu\nabla\boldsymbol{v},$$

where $\boldsymbol{v}$ is flow speed, ρ is the density, p is the preasure and μ is the viscosity, one can use the following SPH discretization [7]:

$$\frac{\mathrm{d}\boldsymbol{v}_i}{\mathrm{d}t} = -\sum_{j\neq i} m_j \left(\left(\sigma_i/\rho_i^2\right) + \left(\sigma_j/\rho_j^2\right) \right) \nabla W_{ij},$$

where $\boldsymbol{v}$ is the velocity field and σ is the stress tensor. We split this expression into two parts, one for the equation of state, the other for the viscous parts:

$$\frac{\mathrm{d}\boldsymbol{v}_i^{\mathrm{pres}}}{\mathrm{d}t} = -\sum_{j\neq i} m_j \left(\frac{p_i}{\rho_i^2} + \frac{p_j}{\rho_j^2} \right) \cdot \nabla W_{ij}$$

$$\frac{\mathrm{d}\boldsymbol{v}_i^{\mathrm{visc}}}{\mathrm{d}t} = -\sum_{j\neq i} \frac{m_j}{\rho_i \rho_j} (\mu_i + \mu_j)(\boldsymbol{v}_i + \boldsymbol{v}_j) F_{ij}.$$

As equation of state, we use

$$p = p_0 \left[\left(\frac{\rho}{\rho_0} \right)^{\gamma} - 1 \right], \qquad \gamma = 7,$$

with which we can specify the allowable density deviation from an incompressible fluid. The sums run both over the fluid particles as well as particles on the wall (see section 5) to model no-slip boundary conditions, with the difference that the particles on the wall remain at their fixed place an thus feel no acceleration. Gravity can be added as constant acceleration term, also a centrifugal pseudo force term depending on the particle's coordinates. For the discretization of the energy equation including stress effects and heat conduction, one can use [7, 8]:

$$\frac{dE_i}{dt} = \sum_j \left[(\boldsymbol{v}_i - \boldsymbol{v}_j) \cdot \frac{\sigma_i}{\rho_i^2} \cdot \nabla W_{ij} - (\kappa_i + \kappa_j)(T_i - T_j) \frac{F_{ij}}{\rho_i \rho_j} \right]. \tag{4}$$

Since during solidification of a metal, heat is released due to the crystallization of the liquid's atoms, a nonlinear $T(E)$ relationship emerges (see, for example, Fig. 3). Thus, the appropriate degree of freedom is enthalpy E instead of temperature T, and functions $T(E)$ are used in (4). Stress effects are expected to be negligible, as is frictional heat, the consequence being that the first term of (4) is neglected.

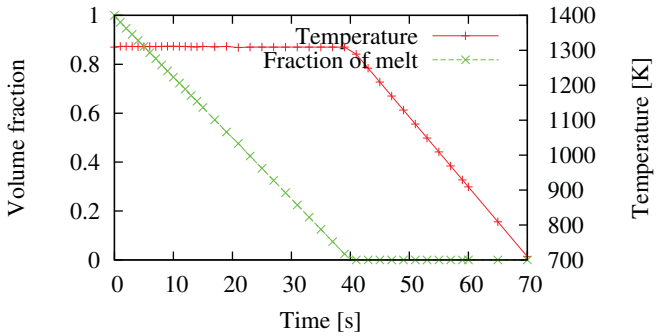

Figure 3: Simulation of the solidification of an CuAl alloy (9 wt-% Al), performed with the microstructure simulator MICRESS[9]: Thermal energy is removed at a constant rate of $50\,\mathrm{J\,cm^{-3}\,s^{-1}}$. Only when the melt is completely solidified and all latent heat is removed does the temperature decrease.

5 Coupling of SPH, FEM and MOR

Coupling is performed through a set of fixed ("wall") particles placed outside of the cavity's boundary, inside the FE mesh. They serve as the slaves in a master/slave coupling setup [10]. To each of those, a small patch l on the boundary is assigned, the patches being chosen based on the expected fluid flow and required spatial resolution (Fig. 4). Each patch gets assigned an input J_l to (2). Heat between fluid particles is exchanged by (4). Heat between fluid and wall particles is also exchanged by this equation, with the modification that the wall particles have an additional temperature DOF, which is determined by solving the reduced system (2); the temperature of the fluid particles is determined only by their enthalpy.

The simulation loop is thus as follows, with i, j being indices for fluid particles and k for wall particles:

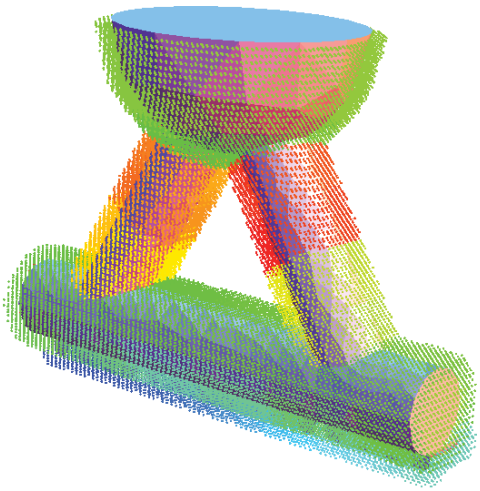

Figure 4: Coupling of wall particles to the FEM system of equations. Different colors signify different input groups.

1. Exchange energy between fluid particles, where the temperature is calculated based on their enthalpy. This allows for phase transitions: $T_{i,j} = T(E_{i,j})$.
2. Exchange energy between wall and fluid particles, where the temperature of the fluid particles is calculated as above and the temperature T_k of the wall particles is calculated from the previous solution of the reduced FEM system.
3. Add up the enthalpies of all wall particles belonging to an input J_l and form the RHS of (2).
4. Update T_k by solving the reduced FEM system.
5. Clear enthalpy DOF of wall particles.

Since the wall particles collect enthalpy, but (2) is written in terms of heat flow, the RHS has to be divided by the timestep. Further, the inputs in (2) are heat fluxes (flow per area); the enthalpies in the wall particles, on the other hand, are already integrated over the necessary area; thus, the columns i of $\mathbf{B}$ in (2) are divided by $\sum_k B_{ik}$.

Time integration of the SPH equations is performed with an explicit velocity verlet algorithm. The reduced FEM system is small enough that the matrices involved can be inverted during the initialization of the software, so that the implicit backward Euler algorithm can be used at each timestep with no performance penalty.

6 Results

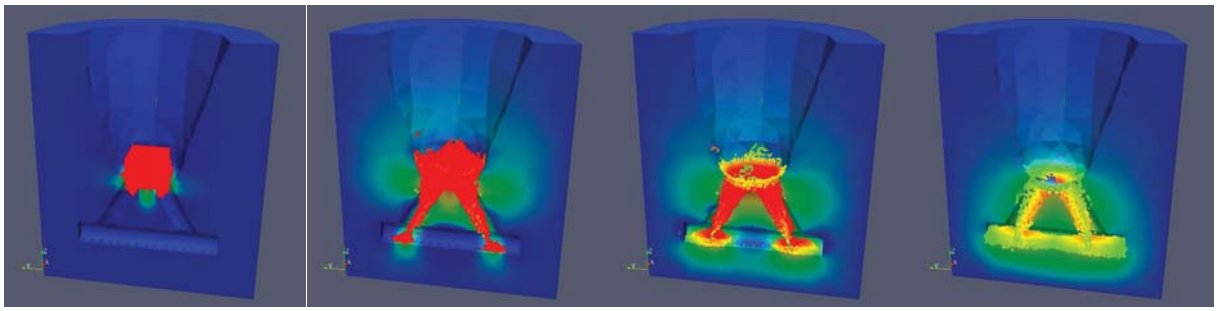

Figure 5: Filling simulation. The fluid's coloring indicates enthalpy, the coloring of the mold indicates temperature.

Figures 5 and 6 show the filling of the mould and the resulting temperature/enthalpy distribution. The heat capacities for mold and fluid have been chosen equal as 1 and as temperature/enthalpy relationship has been set to $T(E) = E$. The cooling of the melt and heating of the mold is clearly visible. The temperature curve shows an interesting feature: The particle is first cooled down as it splashes on the walls, but then warmes up again as it touches other hotter parts of the melt.

The solution of the FEM system, resulting in $O(10^6)$ FLOPs per timestep, is reduced to $O(10^4)$ FLOPs per timestep, which is substantially less than the $O(10^6)$ FLOPs required for the SPH timestep integration.

7 Conclusion

The combination of SPH, FEM and MOR has shown its potential for computationally efficient co-simulation of solid and liquid structure; the CPU time spent to solve the FEM system and even the reprojection overhead is

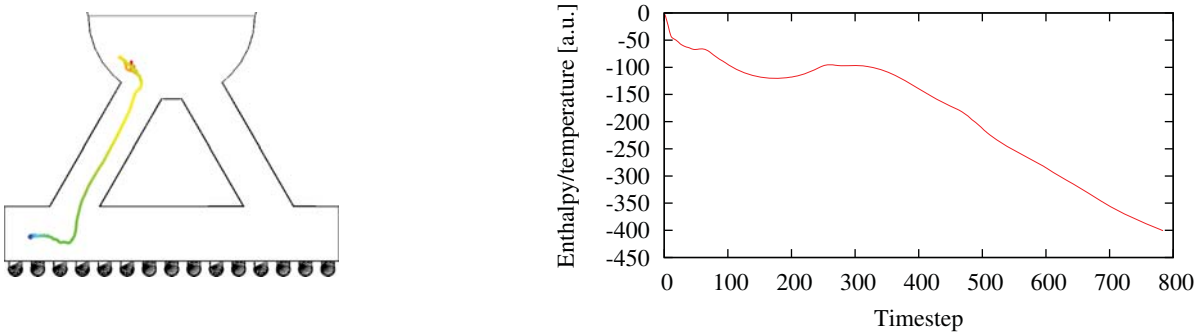

Figure 6: Temperature curve for particle no.1. On the left, the trajectory is shown. It is color coded with the temperature curve shown in the right graph (difference to initial enthalpy shown).

negligible. Comparisons between the simulator running with the FEM solution turned on and off showed no relevant difference in required computing time. The limiting factor is the number and positioning of boundary patches and inputs; more research on many-IO MOR is necessary.

8 Acknowledgments

Funding by the Deutsche Forschungsgemeinschaft, Sonderforschungsbereich Mikrourformen (SFB499) is acknowledged.

9 References

[1] Baumeister, G., Haußelt, J., Rath, S., Ruprecht, R.: *Microcasting*. In: Microengineering of Metals and Ceramics, Wiley VCH, 2005, p. 357–393

[2] Kauzlarić, D., Lienemann, J., Greiner, A., Korvink, J. G., Pastewka, L.: *Integrated process simulation of primary shaping: multi scale approaches*. Microsyst. Technol., 2008. Available online: DOI 10.1007/s00542-008-0612-5.

[3] Lienemann, J., Rudnyi, E. B., and Korvink, J. G.: *MST MEMS model order reduction: Requirements and benchmarks.* Linear Algebra and its Applications, 415 (2006), 469–498.

[4] Antoulas, A. C.: *Approximation of Large-Scale Dynamical Systems, Advances in Design and Control 6*. SIAM, 2005.

[5] Gingold, R. A. and Monaghan, J. J.: *Smoothed particle hydrodynamics: Theory and application to non-spherical stars.* Mon. Not. R. Astr. Soc., 181 (1977), 375–389.

[6] Lucy, L. B.: *A numerical approach to the testing of the fission hypothesis.* Astron. J., 82 (1977), 1013–1024

[7] Randles, P. W. and Libersky, L. D.: *Smoothed particle hydrodynamics: Some recent improvements and applications.* Comput. Methods Appl. Mech. Engrg., 139 (1996), 375–408.

[8] Cleary, P. W. and Monaghan, J. J.: *Conduction modelling using smoothed particle hydrodynamics.* J. Comp. Phys., 148 (1999), 227–264.

[9] ACCESS e. V. MICRESS. [illegible]

[10] Rabczuk, T., Xiao, S. P. and Sauer, M.: *Coupling of mesh-free methods with finite elements: basic concepts and test results.* Commun. Numer. Meth. Engng, 22 (2006), 1031–1065.

[11] Silveira, L. M., Kamon, M., and White, J.: *Efficient reduced-order modeling of frequency-dependent coupling inductances associated with 3-D interconnect structures.* IEEE T Compon Pack B, 19 (1996), 283–288.